Reviewed research article

Polyphase structural evolution of a fine-grained, fold-dominated end moraine, Brúarjökull surge-type glacier, Iceland

Ívar Örn Benediktsson[1,2]

[1]*Institute of Earth Sciences, University of Iceland, Askja, Sturlugata 7, IS-101 Reykjavík, Iceland*

[2]*Department of Geology, Lund University, Sölvegatan 12, S-223 62 Lund, Sweden*

iob2@hi.is, ivar_orn.benediktsson@geol.lu.se

Abstract – *The glaciotectonic architecture and structural evolution of a fine-grained end moraine formed by the 1890 glacier surge of Brúarjökull is described from four excavated cross-sections. The end moraine ridge is a morphological expression of a marginal sedimentary wedge formed during the last days of the surge. The actual end-moraine ridge was formed on the last day of the 1890 surge when the glacier became coupled to the bed and ploughed into the reverse slope of the marginal sediment wedge. Ductile deformation, favoured by high porewater pressure, dominated the construction of the end moraine while brittle deformation was induced when porewater pressure decreased, particularly at the end of the surge. Thus, the deformation was polyphase, developing from open folding to multiple overfolding when porewater pressure was high and finally to overthrusting, faulting and shearing at the very end of the surge when porewater pressure dropped severely upon porewater blow-out in front of the moraine. This structural continuum is exhibited by the four cross-sections. The glaciotectonic stress was absorbed within a relatively narrow zone due to high friction along a basal décollement. A new model illustrates the structural evolution of a fine-grained, fold-dominated end moraine and may serve as an analogue to similar end moraines in modern and Pleistocene environments.*

INTRODUCTION

Glaciotectonic end moraines signify the process of proglacial and submarginal sediment deformation. Thus, the analysis and interpretation of structural features (e.g. folds, faults, shear zones, tectonic fabrics) within them provide important information on influencing factors in the subglacial and ice-marginal environments, and on the thermal and hydrological conditions of the foreland wedge which is deformed to produce the end moraine (e.g. Croot, 1988; van der Wateren, 1995; Boulton *et al.*, 1999; Bennett, 2001; McCarrol and Rijsdijk, 2003; Pedersen, 2005; Aber and Ber, 2007; Phillips *et al.*, 2008; Benediktsson, 2010; Benn and Evans, 2010; Brandes and Le Heron, 2010; Phillips *et al.*, 2011). A number of studies have analysed complex glaciotectonic sequences in Pleistocene (e.g. Thomas, 1984; van der Wateren, 1987, 1995; Pedersen, 2005; Aber and Ber, 2007; Phillips and Merritt, 2008; Parkes *et al.*, 2009; Weaver and Arnaud, 2010) and modern (e.g. Humlum, 1985; Croot, 1987; Krüger, 1994; Hambrey and Huddart, 1995; Boulton *et al.*, 1999; Huddart and Hambrey, 1996; Krüger *et al.*, 2002, 2010; Motyka and Echelmeyer, 2003; Bennett *et al.*, 2004; Kuriger *et al.*, 2006; Benediktsson *et al.*, 2008, 2009, 2010; Roberts *et al.*, 2009) glacial environments in order to elucidate the tectonic development and the glacier-induced processes and stresses involved. This paper contributes a case study to this growing literature based on a fine-grained glaciotectonic end moraine formed by the 1890 surge of Brúarjökull, Iceland. Benediktsson *et al.* (2008)

described the sediment distribution in the marginal zone of the 1890 surge and the architecture and sedimentary composition of the end moraine, and concluded that the moraine was an inseparable part of a marginal sedimentary wedge that was formed during the last few days of the surge. Despite their detailed descriptions, the structural evolution of the actual end-moraine ridge remains to be described. The aim of this paper is therefore to describe the glaciotectonic architecture and the structural evolution of the 1890 end moraine where it consists of fine-grained sediments in Kringilsárrani in the central forefield of Brúarjökull (Figure 1), and thereby linking the moraine directly into the ice-marginal landsystem presented by Benediktsson *et al.* (2008).

SETTING

Brúarjökull is a surge-type outlet of the northern Vatnajökull ice cap in Iceland (Figure 1). It descends from c. 1500 to 600 m a.s.l. and terminates with an approximately 55 km long ice margin (Björnsson *et al.*, 1998). Historical surges occurred in 1625, ∼1730, 1775?, 1810, 1890, and 1963-64, giving a surge cycle of 80–100 years, whereof the active surge phase duration is only about 3 months (Eythorsson, 1963, 1964; Thorarinsson, 1964, 1969; Björnsson *et al.*, 2003). During the last two surges, the glacier advanced 10 and 9 km, respectively, in Kringilsárrani in the central glacier forefield, with maximum ice-flow velocities of at least 120 m/day (Kjerúlf, 1962; Thorarinsson, 1964, 1969; Guðmundsson *et al.*, 1996). During the surges in 1810 and 1890, Brúarjökull advanced further than during previous surge cycles overriding and deforming a sediment sequence of loess, peat and tephra (Benediktsson *et al.*, 2008). The area of Kringilsárrani, in which the central forefield occurs, is a triangular area bounded by the glacier to the south, and the glacial rivers Jökulsá á Dal and Kringilsá to the east and west, respectively (Figure 1).

The Brúarjökull forefield is glacially streamlined with a 6–7 m thick sediment sequence overlying basaltic bedrock. The most prominent landforms of the forefield are end-moraine ridges, ice-cored landforms and ice-free hummocky moraine, crevasse-fill ridges, eskers, concertina eskers, and flutings (Evans and Rea, 1999, 2003; Kjær *et al.*, 2006, 2008; Schomacker *et al.*, 2006; Evans *et al.*, 2007; Schomacker and Kjær, 2007; Benediktsson *et al.*, 2008, 2009) (Figure 1). At present, there is negligible ice movement in the marginal 1–2 km of Brúarjökull and the snout is rapidly retreating and downwasting (Kjær *et al.*, 2008).

METHODS

The sedimentology and glaciotectonic architecture of the 1890 end moraine in Kringilsárrani were investigated in four natural cross-sections that were cleaned and enlarged by hand. Sediment lithologies and structures were documented on the basis of the data chart by Krüger and Kjær (1999) and deformation structures were described according to the terminology of Twiss and Moores (1992) and Evans and Benn (2004). The glaciotectonic architecture was mapped at a scale of 1:20 and structural elements, such as strike and dip of primary bedding and fault planes and plunge and direction of fold axes, were plotted and statistically analysed in a Schmidt equal-area net with the SpheriStat 2.2 software.

Line and area balancing were applied to the four cross-sections to calculate the horizontal shortening of the sedimentary strata and the depth to the décollement plane (Marshak and Mitra, 1988; Benediktsson *et al.*, 2010). By tracing tephra marker horizons through the sections and measuring the horizontal (shortening) distance which they occupy, the difference (ΔL) between their length in the undeformed (L_u) and deformed (L_d) states could be determined. Then the total shortening is described as: s = L_d–L_u / L_u. By calculating the total area of the deformed section (A), the décollement depth can be estimated by: h = A / ΔL. Then it is assumed that the area of the body subjected to stress remained constant before (Au) and after (Ad) deformation. The tephra marker horizons were visually traced through each section on the basis of their general appearance and properties (particularly grain size and colour) and stratigraphical position. It should be noted that tracing the tephra markers through the sections often requires inferences as to where and how different marker segments connect. The inferences made are conservative and there-

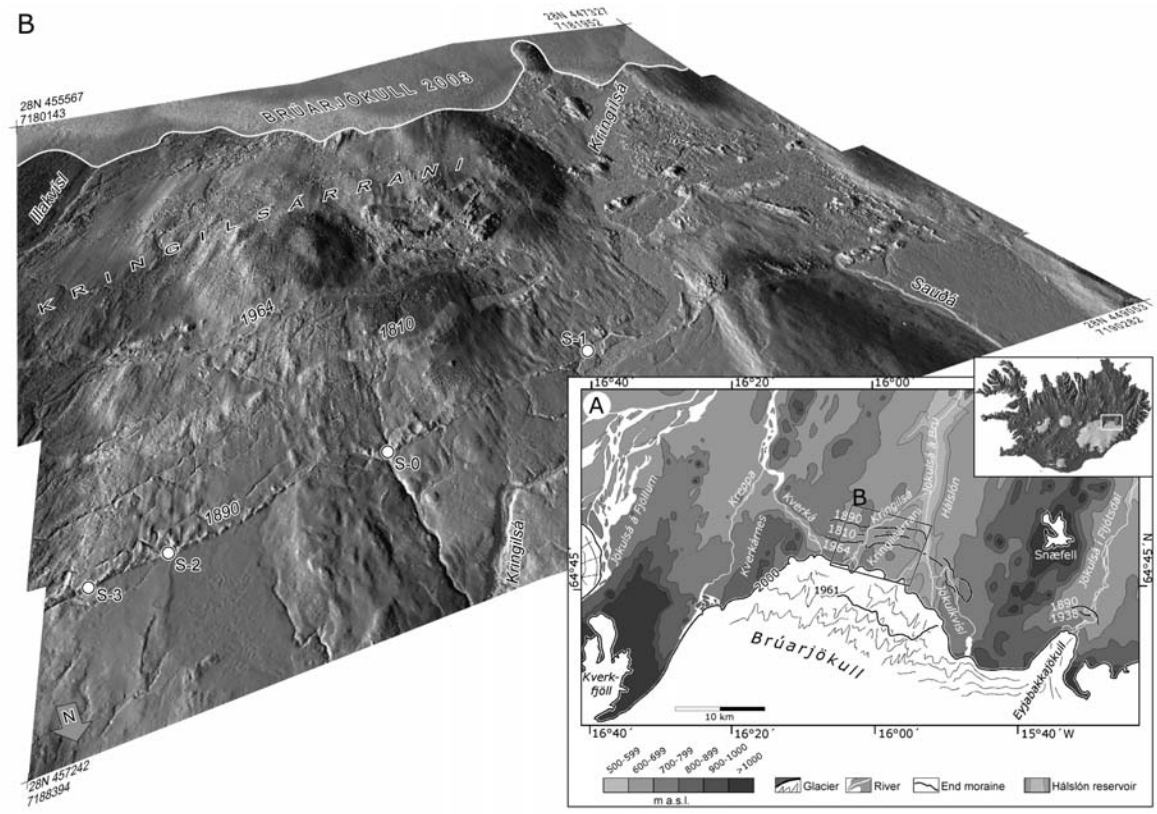

Figure 1. A) The location of Brúarjökull at the northern margin of the Vatnajökull ice cap in Iceland. B) Digital elevation model of the central forefield of Brúarjökull in Kringilsárrani. Points S-0 to S-3 indicate excavated cross-sections in the 1890 end moraine. The area is approximately 8 km across. UTM coordinates are in metres. *– A) Kort af rannsóknasvæðinu við sporð Brúarjökuls. B) Hæðarlíkan af framlandi Brúarjökuls í Kringilsárrana. Punktar S-0 – S-3 tákna þversnið sem kortlögð voru í jökulgarðinum frá framhlaupinu 1890. Jökulgarðar framhlaupanna 1810 og 1964 eru einnig merktir. Svæðið er um 8 km í þvermál. UTM hnit eru í metrum.*

fore, the numbers obtained on the horizontal shortening and décollement depth can be regarded as minimum and maximum numbers, respectively.

THE 1890 END MORAINE AS A PART OF A DUAL MARGINAL LANDFORM

During the 1890 surge, the ice was coupled to the overall fine-grained bed, as evident from strong clast fabric in flutes and significant subglacial deformation (Kjær *et al.*, 2006). Overpressurized porewater in the substrate lowered the effective pressure and favoured decoupling at the substrate-bedrock interface, as indicated by laminated dewatering structures that drape the bedrock surface but unconformably truncate the overlying layers of the substrate (Kjær *et al.*, 2006). Due to the decoupling, the substrate was dislocated downglacier, resulting in high sediment influx to the marginal zone. During the downglacier transport, the subglacial sequence was deformed compressively through multiple folding. To accommodate the sediment surplus in the marginal zone, a ∼500 m long

sediment wedge, in which the sediment thickness increases from 1–3 m at the upglacier end to >7 m at the end moraine crest, was formed (Benediktsson *et al.*, 2008; Figure 2). By comparing the length of the wedge and observed ice-flow velocities (∼120 m-day) from the 1963-64 surge of Brúarjökull, Benediktsson *et al.* (2008) deduced that the wedge was formed in about five days. Moreover, they claimed that the 1890 end moraine formed on the distal top of the wedge during the last day of the surge, approximately, in response to a drop in submarginal porewater pressures following blow-out of overpressurized water in front of the glacier. Thus, the sediment wedge and the end moraine form a dual, inseparable marginal end product of the 1890 surge (Figure 2). A detailed description of the structural evolution of the end-moraine ridge has not been given before and follows below.

GEOMORPHOLOGY, SEDIMENTOLOGY AND INTERNAL ARCHITECTURE OF THE 1890 END MORAINE

Apart from low and narrow dump moraines in areas of elevated bedrock and thin sediment cover, the 1890 end moraine in Kringilsárrani is 5-20 m high and 40-80 m wide and most prominent in topographic depressions where the sediment cover is thick (Figure 1). Usually, the foreslope is steep and the backslope gentle with ice-free hummocky moraine. Active downwasting of buried ice is rare where the moraine consists of fine-grained sediments (Schomacker and Kjær, 2007; Benediktsson *et al.*, 2008). The internal sedimentary composition and architecture of the 1890 end moraine was studied in four cross-sections. Five sediment facies were identified; F1 diamict, F2 gravel, F3 interbedded sand and silt, F4 deformed LPT, and F5 tephra. F4 and F5 are most dominant and occur in all sections while F1, F2, and F3 were found in two sections. Descriptions and interpretations of the sediment facies follow in Table 1. Three of the sections (1–3) were described by Benediktsson *et al.*, 2008 but are now revised. Two new sections are added and described for the first time; section 0 and sub-section 2a.

Section 0

Section 0 is located in the central part of the 1890 end moraine in Kringilsárrani (Figure 1) along a small stream running on bedrock. This stream occupies a

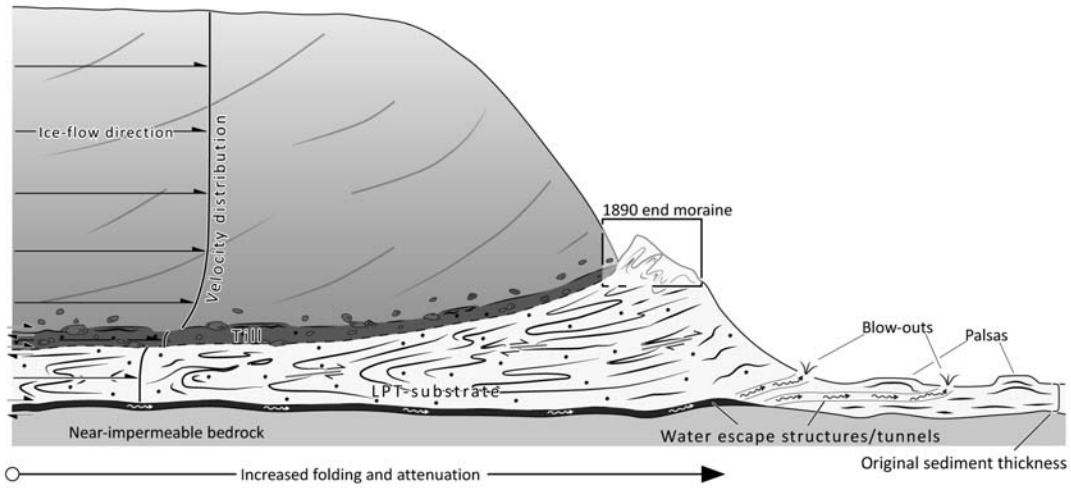

Figure 2. Conceptual model illustrating the formation of the marginal sediment wedge with the actual end-moraine ridge on the distal top. See text for details. Modified from Benediktsson *et al.*, 2008. – *Líkan sem sýnir myndun setfleygs undir sporði Brúarjökuls á síðustu dögum framhlaupsins 1890. Sjálfur jökulgarðurinn myndaðist á toppi fleygsins á síðasta degi framhlaupsins.*

Table 1. Sedimentary facies identified in the 1890 end moraine in Kringilsárrani. – *Setásýndir í jökulgarðinum frá 1890 í Kringilsárrana.*

Facies	Location and description	Interpretation	References
F1	Section 1 – up to 60 cm thick but discontinuous massive, silty-sandy to sandy, matrix- supported, clast-rich, friable diamict. Contact to underlying facies 2 is sharp and possibly erosional. Clasts are <10 cm with similar shapes as in underlying facies 2 and rare or non-preferred striae orientation. The diamict interfingers with facies 4.	Till – pre-surge till of unknown age, deposited at the interface between the ice and an under- lying sandur surface (facies 2). Clasts from the sandur were incorporated into the diamict in a deforming-bed.	Eyles et al., 1983; Krüger and Kjær, 1999; Benn and Evans, 2010.
F2	Section 1 – massive, clast-supported gravel, with pebbles of 3–8 cm although outsized pebbles of 15–20 cm occur. Clasts are sub-rounded to rounded, elongated in shape and often imbricated.	Sandur – deposited prior to the 1890 surge during moderate meltwater discharge. Represents a low-lying terrace formed during a down-cutting of the Kringilsá river. Genesis is evident from the surface morphology of sandur terraces around the section.	Maizels, 1993; Benn and Evans, 2010.
F3	Section 2 – faintly stratified, dark-brown, dark-gray and ligh-brown layers of fine to coarse sand, interbedded with thin (1-10 mm) silty layers of facies 4 and containing some organic matter (which is often rusty and give yellowish hue). Contacts to facies 4 are sharp, erosive and defined by normal faults on distal side.	Shallow pond or stream sediments – resemble sediments found in channels and circular lakes (collapsed palsas) proximal and distal to section 2, respectively, where organic matter is abundant.	French, 1996; Maizels, 2002.
F4	Sections 0–4 – 0.1–2 cm thick clay, silt and fine-sand laminae of yellowish to orange and red-brown peat and light-brown to dark-brown loess interbedded with tephra. Laminae thickness and strength varies greatly within different tectonic regimes. The facies constituents are totally mixed in places. Contacts between laminae are usually sharp but may be gradational.	Loess-peat-tephra sequence (LPT) – cohesive sequence of loess, peat and tephra. Peat formed from the submergence of vegetated terrain (mosses and grasses) during loess aggradation. The vertical accretion of loess and peat was frequently interrupted by depostion of tephra. The sequence was formed prior to the 1890 surge.	Brady and Weil, 1999.
F5	Sections 0–4 – generally 0.5–3 cm thick layers of black basaltic and white to yellowish rhyolithic tephra with <2 mm angular grains. Thickness varies grately and is the most (<10 cm) in association with folds. The tephra either occurs in continuous or discontinuous layers, or as pathces or lenses, particularly within facies 4.	Tephra – primary air-fallen (not redeposited), transported by wind from various Icelandic volcanoes. White tephra marker is from Öræfajökull AD1362.	

minor meltwater outlet of the 1890 surge (Figure 3). In this area, the 1890 end moraine is generally 70 m wide and 10 m high with a steep frontal slope and a hummocky backslope. However, the particular ridge segment in which section 0 occurs is 15–20 m wide and approximately 5 m high. Section 0 is 3 m wide and 2.7 m high and covers the core of the ridge but is orientated at a 45° angle to the ridge strike (Figure 3). Two sediment facies were identified in the section: deformed LPT (F4) and tephra (F5) (Table 1). The section is described from bottom up.

The base of the section, i.e. the lowermost ∼80 cm, is characterized by sub-horizontal, continuous tephra layers and LPT beds which develop upwards into discontinuous lenses and patches as they approach the core of a north-verging recumbent syncline. This is signified by the white Öræfajökull AD 1362 tephra marker. The core of the fold contains occasional tectonic foliation. The upper limb of this syncline forms the lower limb of a north-verging recumbent anticline, as revealed by the LPT beds and tephra layers which are overall thin on the limbs but thicken

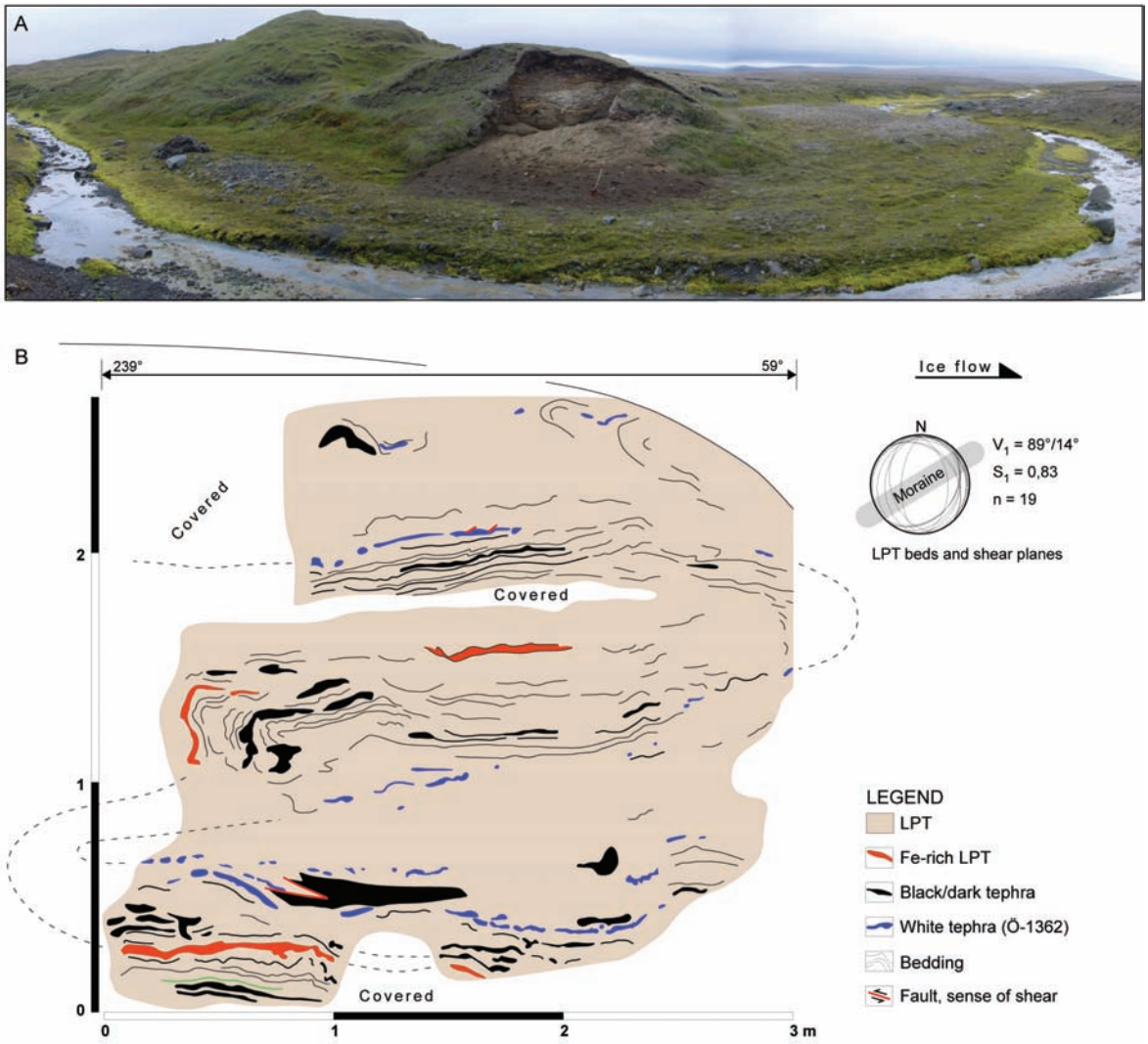

Figure 3. Section 0. A) Photograph of the section. B) Drawing of the section. Structural data to the right. Ice flow from left to right. V_1 denotes the principal eigenvector, S_1 is the eigenvalue (strength between 0 and 1) of that vector, and n number of measurements. – *A) Ljósmynd af sniði 0 og B) teikning af sniðinu. Grafið til hægri sýnir þrívíða legu setlaga og misgengja. V_1 táknar meðalstefnu og halla, S_1 táknar tölfræðilegan styrk reiknaðra meðaltala og n táknar fjölda mælinga. Þrýstingur jökuls frá vinstri til hægri.*

considerably in the hinge zone of the fold. The upper part of the section is dominated by sub-horizontal layers that form the upper limb of the north-verging anticline (Figure 3).

By tracing the LPT beds and tephra layers through the section, and in particular, the white Öræfajökull AD 1362 tephra marker, it is possible to reconstruct a large, recumbent, north-verging anticline-syncline

pair, which has a general plunge to the east (Figure 3). Patches of the Öræfajökull AD 1362 tephra near the surface can possibly be connected to the same tephra layer approximately 0.5 m below via another proximal recumbent syncline. Balancing of the section, with fold hinges inferred, shows that the minimum horizontal shortening is 6 m or 67%, and that the décollement surface lies at 1 m depth, which coincides with the bedrock surface at the base of the section. The strike and dip of the principal plane (89°/14°N) confirm that stresses were induced from the south (Figure 3). This particular segment of the 1890 end moraine indicates that the glacier coupled to the foreland at least a few metres upglacier from its terminal position and deformed the foreland strata into an open fold that subsequently overturned.

Section 1

Section 1 is located along one of the major meltwater outlets of the 1890 surge (Figure 1), now occupied by the Kringilsá River. The moraine ridge is 20–25 m wide here and 1.5–2.5 m high and symmetric in shape (Figure 4). Section 1 is orientated approximately perpendicular to the moraine strike. Four sediment facies were identified: diamict (F1), gravel (F2), LPT (F4), tephra (F5) (Table 1). A sub-horizontal gravel bed (F2) underlies the entire section and forms a décollement. Above this bed, the sediments are deformed. Based on the style and magnitude of glaciotectonic deformation, the facies architecture can be divided in three parts: (i) the proximal part (0–3 m), (ii) the central part (3–15 m), and (iii) the distal part (15–22 m).

Proximal part, 0–3 m.

The proximal part is characterized by deformed pre-surge diamict which interfingers with LPT, in particular. The LPT includes boudinaged and small-scale folded sand, indicative of both tensile and compressive stresses, but is otherwise crudely bedded and contains few sedimentary and deformation structures, mainly due to destruction by roots in the upper levels (Figure 4).

Central part, 3–15 m.

This part of the section reveals the heaviest glaciotectonic deformation in the end moraine. The moraine is characterized by shear zones, frequent small scale folds, and foliation (Figure 4). A number of recumbent and inclined folds exist in the lower core. For example, just above the gravel bed at 3–5 m there are small overturned and recumbent folds with axial dips to north and south and vergence to west and southwest, respectively, indicating principal stress application from easterly directions (Figure 4D). In many places of the lower central part, but particularly at 10–13 m, the different sediment facies have been homogenised by continuous deformation (van der Wateren 1995) and therefore contain no sedimentary or deformation structures. A shear zone occurs above the lower central part and is typified by non-periodic asymmetric box folds verging north, and attenuated sheath folds verging west (Figure 4C). This shear zone marks the lower boundary of an anticline-syncline pair that overrode the lower part. The anticline-syncline pair is asymmetric in the sense that the anticline is considerably wider than the syncline. Measurements on the syncline show that the proximal and distal limbs dip steeply towards north-west and southwest indicating that the syncline closes towards west. The dip of the sedimentary beds of the anticline could not be measured due to poor accessibility.

Distal part, 15–22 m.

This part of the section is dominated by deformed pre-surge diamict (F1) in the lower part but sand and silt (F3), LPT (F4), and tephra (F5) in the upper part. The diamict interfingers with the other sediment facies but attenuates in the distal extremity of the section. Above the diamict, there are minor overturned folds at 14–16 m and thrusts at 17 m which indicate that there is an overturned anticline that has been thrust up in front of the syncline (Figure 4). Apparently, the hinge of this anticline has been either truncated by syn-tectonic slope failure or eroded by syn- or post-tectonic meltwater. Soil and roots at the surface prevented this to be further determined. Distal to the minor thrusts there is open folding of LPT and gravel that fades out and merges imperceptibly with the undeformed sandur in the foreland (Figure 4).

The deformation in section 1 can be divided in three phases. It commenced with folding and, to a lesser extent, thrusting, of the foreland strata in front

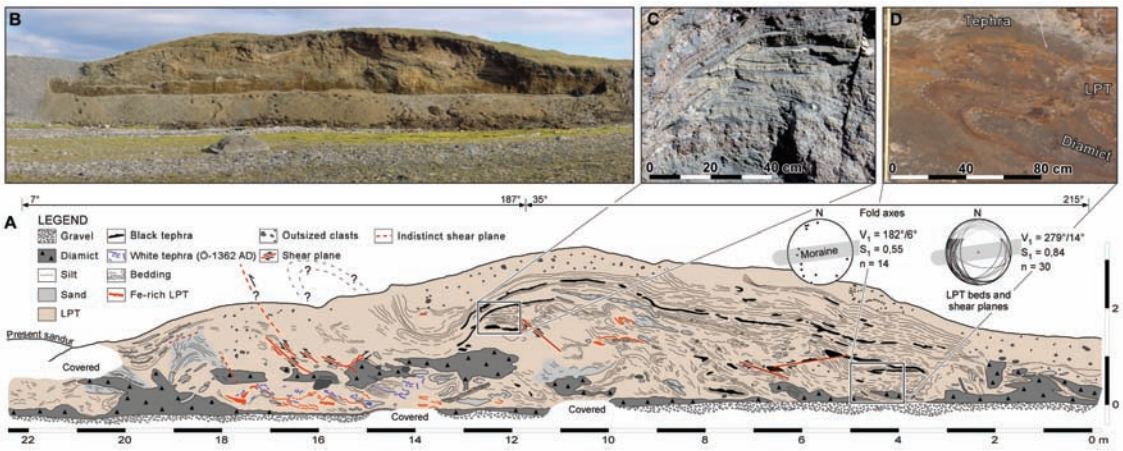

Figure 4. Section 1. A) Detailed drawing of the section with structural data. B) Photograph of the section. C) Tectonically foliated sheath folds in the section core. D) Recumbent folds in the proximal part of the core. Ice flow from right to left. *– A) Teikning af sniði 1. Gröfin sýna þrívíða legu setlaga, misgengja og fellingaása í sniðinu, sjá skýringar við 3. mynd. B) Ljósmynd af sniði 1. C) Hringlaga slíðursfellingar og D) liggjandi fellingar í kjarna garðsins. Þrýstingur jökuls frá hægri til vinstri.*

of the advancing ice. As the pressure from the glacier increased, the uppermost strata sheared over the strata below to form the asymmetric box and sheath folds and the anticline-syncline pair, which constitutes the ridge form of the end moraine. Simultaneously, the lower part below the shear zone deformed further and became largely homogenised, and a new anticline formed in front of the syncline. Subsequently, this new anticline overturned and thrust over slightly folded strata in the distal part before the deformation ceased.

The upwards decrease in strain in the central part of the section is consistent with variable amounts of horizontal shortening. While the layers of the asymmetric box folds in the shear zone below the anticline have been shortened by 46%, the upper strata forming the anticlines and synclines have been shortened by 23%. If the depth to the basal décollement is calculated on the basis of these numbers, the depth to the basal décollement would be 5–9 m. These numbers do not correspond to the surface of the gravel body at the base of the section and indicate a somewhat deeper deformation at this site than previously suggested (Benediktsson *et al.*, 2008) and that the gravel body was indeed incorporated in the deformation. The large differences in horizontal shortening within the section reflect contrasting strain accommodation within the sediment pile, likely indicating polyphase deformation of the foreland. The structural data within section 1 show that fold axes are dispersed and barely reliable indicators of the direction of stress, while LPT beds and faults strongly suggest stress application from the south, as expected (Figure 4).

Sections 2a and 2b

Sections 2a and 2b are located in the eastern part of the central forefield in Kringilsárrani (Figure 1) in a wind eroded trench that exposes the central part of the end moraine. Three sediment facies were recognized in the sections; interbedded sand and silt (F3), LPT (F4), and tephra (F5) (Table 1). Section 2a has not been described before and gives an insight into the architecture of the backslope of the end moraine and the glaciotectonic processes operating beneath or just in front of the ice margin. Section 2b, which covers the proximal to distal core of the moraine, was previously described by Benediktsson *et al.* (2008). Their descriptions are slightly revised here. The end moraine is up to 10 m high and 50 m wide at this site.

Section 2a, the backslope.

This section is almost 3 m high and 12 m wide and covers the backslope of the moraine at this site (Figure 5). It is situated opposite to section 2b in the abovementioned trench that penetrates the moraine. A prominent listric thrust fault characterizes this section and cross-cuts folded layers. The layers of the hanging wall, outlined by 3–4 prominent tephra markers, dip 14–40° towards the south. Several small-scale inclined and recumbent overturned folds with vergence to the north occur immediately above the thrust and occasional boudinage structures are also found in the tephra layers. Higher with the section, the deformation is less, as exemplified by the continuous and undisturbed white Öræfajökull AD 1362 tephra marker horizon near the surface. At ca. 3–8 m in the footwall of a thrust fault, the deformation is similar to that of the lower part of the hanging wall with small scale folds. A thick layer of black tephra is observed in the footwall near the surface at 6–7 m. Most likely, this tephra layer correlates with the black tephra layers in the hanging wall, thereby giving a displacement along the thrust fault of ca. 1 m. At 5–8 m in the footwall of the thrust, a linear structure was observed which could possibly indicate another thrust fault. However, this is difficult to determine due to indistinct bedding in this area of the section and the thrust's unexposed footwall. At around 10 m, boudins in the white Öræfajökull AD 1362 tephra marker and LPT bedding indicate a synclinal structure, which potentially relates to an overturned fold that connects to the footwall of the aforementioned prominent thrust fault (Figure 5).

Section 2b, the proximal part, 0–11 m.

The upper part is characterized by slightly deformed LPT and tephra layers forming the hanging wall of a low-angle normal fault at ca. 2–6 m (Figure 6). The footwall of this normal fault is dominated by compressive deformation as indicated by small-scale open, inclined, and recumbent folds and back-thrusts. Normal faults also occur and relate either to the shearing of the upper strata across the lower part, or to settling when compression ceased. Two

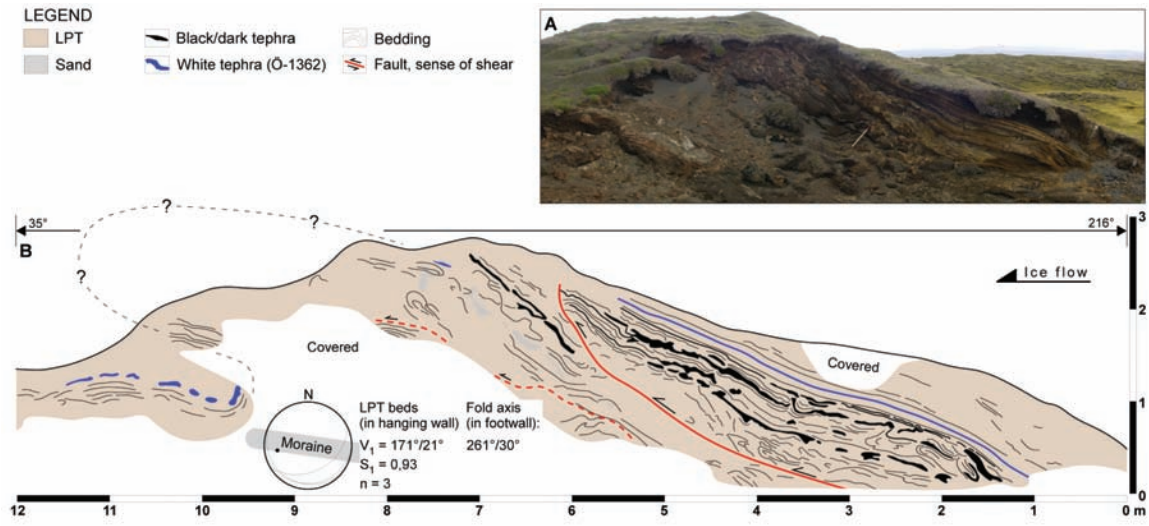

Figure 5. Section 2a. A) Photograph of the section in the proximal part of the end moraine. B) Drawing of the section with structural data. Ice flow from right to left. – *A) Ljósmynd af sniði 2a í innri hluta garðsins. B) Teikning af sniði 2a. Grafið sýnir þrívíða legu setlaga og eins fellingaráss í sniðinu, sjá skýringar við 3. mynd. Þrýstingur jökuls frá hægri til vinstri.*

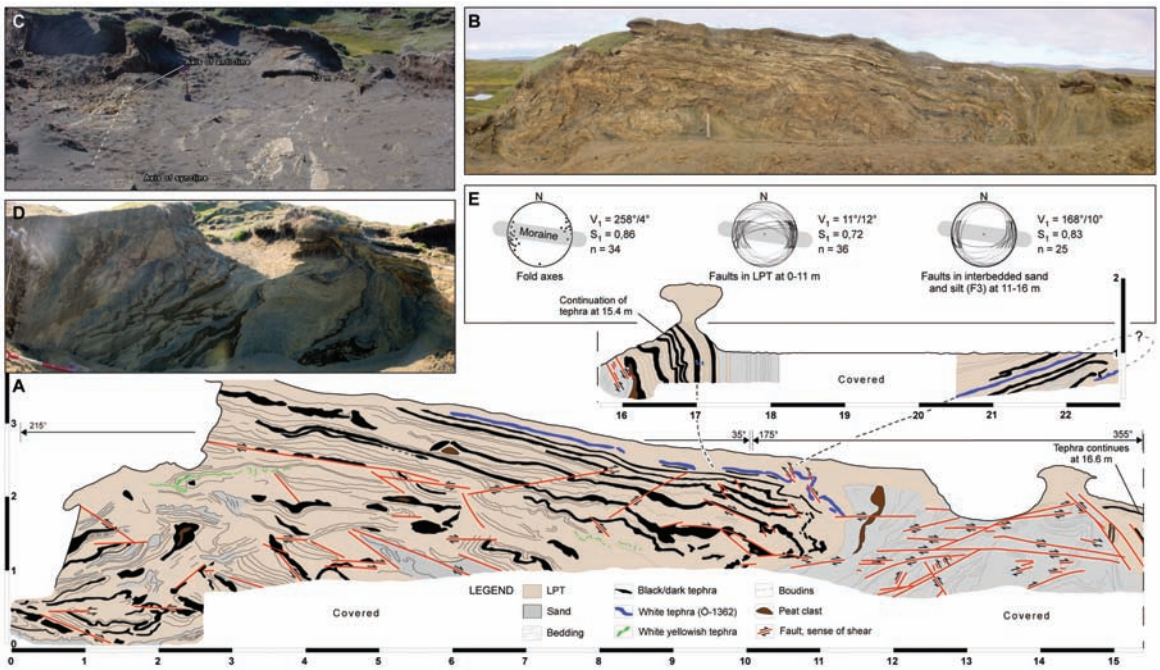

Figure 6. Section 2b. A) Drawing of the section. B) Photograph of the proximal and central core. C) Axes of an anticline and a syncline exposed on the surface in the distal part. D) The central core with frequent faults and shears. E) Structural data. – *A) Teikning af sniði 2b. B) Ljósmynd af sniðinu. Á myndina vantar þó ysta hlutann. C) Mynd sem sýnir ása samhverfu og andhverfu í ytri hluta garðsins. D) Miðhluti sniðsins sem samanstendur af sandi og silti og er alsettur smáum misgengjum. E) Gröf sem sýna þrívíða legu fellingaása og misgengja í sniðinu, sjá skýringar við 3. mynd. Þrýstingur jökuls frá vinstri til hægri.*

prominent thrust faults dipping 27–35° W were observed at 6-9 m. Fault-propagation folds occur along these thrusts, indicating flexural bending of the layers in advance of the actual rupture and development of the fault planes. At 9–11 m, small-scale overturned folds (ductile thrusts) can be observed in the upper part. Small-scale backthrusts, particularly in the white Öræfajökull AD 1362 tephra marker, are associated with the overturned folds and probably indicate an obstruction in front that interrupted the folding (Figure 6). Structural data show preferred dip of fault planes to the north, indicating that most of the faults observed in this part of the section are normal faults and backthrusts.

Section 2b, the central part, 11–16 m.

The central part consists of a fault zone in interbedded sand and silt (Figure 6). The sand and silt beds outline an inclined, east-verging anticline between 14 and 15 m. The upper and lower limbs of this anticline have been cross-cut by several small-scale thrust faults, most of which are low-angle thrust faults dipping towards the south-west to south-east. Steeply dipping backthrusts also occur, particularly at 12–13 m in the lower part and around 15 m in the upper part, cross-cutting folded layers of the interbedded sand and silt. Measurements of the faults in this part of the section show southward dip of the faults and strongly indicate pressure from the south.

Section 2b, the distal part, 16–23 m.

This part of the section is dominated by an asymmetric north-verging fold. This is indicated by anticlinal and synclinal structures observed on the surface by the section foot (Figure 6). The hinge of the anticline is visible in the section at around 16 m. At 16–17 m, near-vertical layers of LPT, sand, and tephra constitute the distal limb of the anticline and the proximal limb of the syncline in front, the hinge zone of which is buried. At 20-23 m, the section is characterized by gently dipping layers of LPT, sand, and tephra, indicating the distal limb of the syncline. Repetition of tephra layers at 22–23 m indicates an overturned fold, the hinge of which can be inferred (Figure 6). The east-west orientation and westward plunge of the fold axes at 16–17 m indicates stress application from the south.

Section 2 shows 3–4 separate phases of deformation. Initially, compressive deformation took place producing small-scale folds which are visible in the lower proximal part of the section. Continued pressure from the ice forced the shearing of the upper strata across the lower part to form an open anticline. The shearing is implied by normal faults in the proximal part. Simultaneously, a syncline formed in front of this anticline and a second, overturned anticline in the distal part. The final deformation phase included thrust faulting within the proximal open anticline.

Line balancing of the tephra marker horizons reveals different amounts of horizontal shortening through the section and gives minimum numbers for it. While layers in the upper part of the proximal core (at ca. 2–11 m) have been shortened by about 9%, the layers in the distal core have been shortened by 30%. By ignoring the interbedded sand and silt at 11–16 m and inferring the hinges of the syncline at 17–20 m and the overturned fold at ca. 23 m, the minimum horizontal shortening in the entire section is calculated as 20%. Calculations of the décollement depth require data on the cross-section area. Due to wind erosion, however, the section outline does not reflect an ideal cross-section through the moraine ridge, and thus it was not deemed relevant to calculate the section area and the depth to the décollement at this site.

Section 3

Section 3 is situated in the easternmost part of the central forefield in Kringilsárrani (Figure 1), along an abandoned minor meltwater outlet channel of the 1890 surge. The end moraine is up to 15 m high and 30–50 m wide at this site, but is considerably higher and wider further to the east and lower and narrower to the west. The proximal slope is hummocky and steep while the distal slope is smooth and gentle. In front of the moraine at this site, the terrain is dominated by circular rim ridges, indicating collapsed palsas, and abruptly emerging channels that represent blow-out of overpressurized water at the end of the 1890 surge (Kjær *et al.*, 2006; Benediktsson *et al.*, 2008). Section 3 covers the core and the distal slope of the moraine (Figure 7). The proximal part and the backslope are not exposed.

Three sediment facies were identified in section 3: interbedded sand and silt (F3), LPT (F4), and tephra (F5) (Table 1). The section is characterized by primary multiple folding and secondary faulting. The section is divided in three parts: (i) a section that subparallels the moraine ridge (0–2 m), (ii) the core (0–9 m), and (iii) the distal slope (9–12.7 m).

Section sub-paralleling the moraine ridge, -0–2 m.

In this section, inclined folds are observed in LPT beds and the white Öræfajökull AD 1362 tephra marker. Repetition of the tephra marker probably indicates the limbs of multiple folds, the hinge zones of which can be identified in the central part of section 3. The limbs of the folds dip towards the abandoned channel at the foot of the section and are frequently sheared by both low- and high-angle faults, two of which are normal faults that indicate syntectonic slope failure during the moraine-ridge formation. A high-angle thrust fault in the upper part, dipping 46° SE, correlates with a thrust fault in the upper proximal part of the main section (Figure 7).

The central part, 0–9 m.

The central part of section 3 reveals the most intense deformation with multiple folding and prevalent faulting (Figure 7). The faulting is most intense between 0 and 4 m with both high-angle and low-angle normal and thrust faults. This is exemplified by e.g.

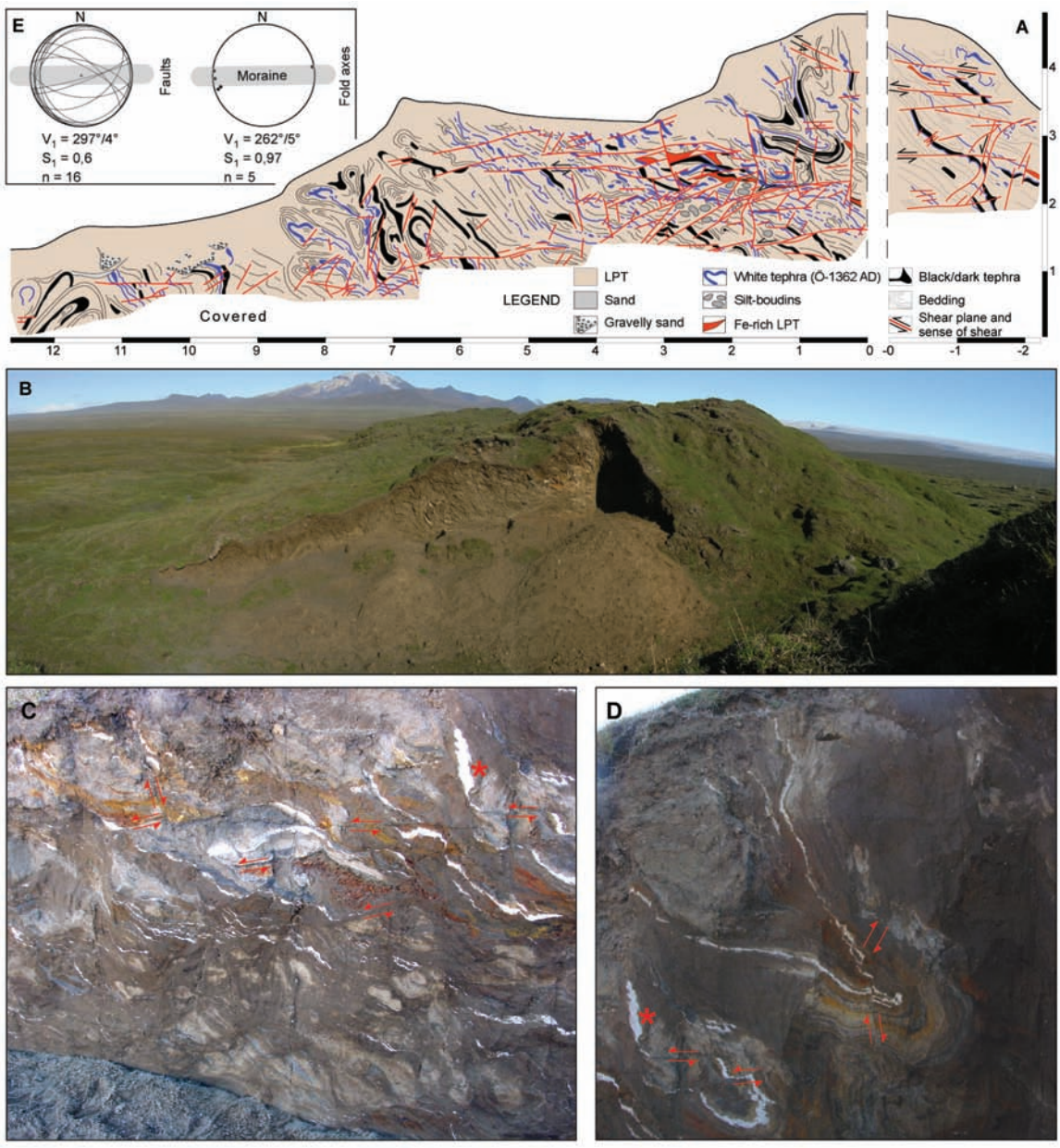

Figure 7. Section 3. A) Drawing of the section. B) Photograph of the section in the central and distal part of the end-moraine ridge. C) Multifolded and faulted core of the moraine. D) Polyclinal folds in the core. The asterisks on C and D denote the same spot. E) Structural data. – *A) Teikning af sniði 3. B) Ljósmynd sem sýnir staðsetningu sniðsins í jökulgarðinum. C) Fellingar og misgengi í kjarna garðsins. D) Fjölhalla yfirfellingar og lítil misgengi í kjarna garðsins. Stjarna á myndum C og D er á sama stað í sniðinu. E) Gröf sem sýna þrívíða legu misgengja og fellingaása, sjá skýringar við 3. mynd. Þrýstingur jökuls frá hægri til vinstri.*

a few high-angle normal faults at 1–3 m that dip 80-85° S, a high-angle backthrust at ∼7 m dipping 75° NE, and a number of low-angle normal faults, particularly in the lower part (below 3 m) (Figure 7). The most prominent structures in the central part are large north verging, overturned polyclinal folds at 0–2 m with upglacier dipping axial planes. The white Öræfajökull AD 1362 tephra marker, LPT beds, and tephra layers outline the fold axis which plunges 8° W. The abovementioned high-angle normal faults cross-cut the folds as do thrust faults in the upper part that correlate with the thrusts described from the section at 0–2 m (Figure 7). At ca. 1 m, the white tephra outlines another prominent fold but its limbs are not easily identified due to intense faulting. From 4 to 6 m, there are upglacier inclined beds of LPT and tephra that are repeated upwards. These beds are thought to represent multiple fold limbs while the fold hinges have either been eroded away (above) or are buried (below). In the upper part at 6–9 m, there are a number of inclined, north-verging folds with shallow axial plunge towards west. The limbs and hinges of these folds are commonly cross-cut by high-angle normal faults and backthrusts, some of which are slightly folded and thus indicating fault formation before folding was completed.

The distal slope, 9–12.7 m.

The most dominant structures in this part of the section are fairly steeply inclined, south verging folds with axes plunging 4° towards east. This is typified, in particular, at around 12 m where black tephra and LPT beds outline the folds. The fold vergence to the south suggests an obstacle in front of the moraine that created a counter-stress from the north during the moraine-ridge formation.

The deformation in section 3 probably initiated in a similar manner as in sections 0, 1, and 2, i.e. with small-scale folding of the lower strata and subsequent open folding and shearing of the upper strata across the lower part. It is suggested that sections 3 represents the most developed stage in the end moraine formation with an additional phases of multiple folding and faulting before the deformation ceased. The main faulting phase occurred towards the end of the moraine formation. This is evident from frequent cross-cutting by faults through folds. However, slightly folded fault planes indicate that faulting commenced shortly before folding ceased.

Steeply dipping normal and thrust faults are common in section 3. They show little consistency in terms of orientation although the principal vector plots as dipping towards WNW. Although the orientation of only five fold axes could be measured directly, they show remarkably strong east-west orientation, which corresponds to stress induced from the south or north. Thus, the fold axes seem to be a more reliable structural indicator of the direction of stress than faults (Figure 7). The general steepness of both folds and faults in the section indicates that the folds are rooted and that the glaciotectonic stress was absorbed within a relatively narrow zone bounded by the glacier to the south and permafrost to the north.

Due to the multiple folding and intense faulting, in particular, it is very difficult to trace marker horizons through the section. Therefore, it is impossible to apply line and area balancing to the entire section 3. However, and just to get a glimpse of the total horizontal shortening at this site, line balancing was applied to the polyclinal folds at 0–2 m, through which the tephra marker horizons could be followed. This revealed a horizontal shortening of 76%, which, because of the common refolding in the section, must be considered to be fairly representative for the moraine ridge at this site.

POLYPHASE STRUCTURAL EVOLUTION OF THE 1980 END MORAINE

Together with a marginal sediment wedge, the 1890 end moraine forms a dual, marginal end product of the 1890 surge (Benediktsson *et al.*, 2008). Much of the deformation observed in the end-moraine ridge, particularly in the proximal part, can be regarded as part of the wedge formation, and the basal décollement must therefore be common for these two ice-marginal components (Benediktsson *et al.*, 2008). The four sections in the end moraine reveal different styles and magnitudes of deformation and by studying the morphology of the 1890 end moraine, Benediktsson *et al.*

(2008) identified a positive relationship between the size of the end moraine and the magnitude of deformation. Section 3 exposes the largest parts of the 1890 end moraine and shows by far most strain whereas section 1 occurs in a low ridge and reveals the least strain. These two can therefore be regarded as end members in a structural continuum of the 1890 end moraine. Sections 0 and 2 connect the two end members with intermediate strains and deformation styles that to some extent resemble those observed in sections 1 and 3.

As concluded by Benediktsson *et al.* (2008), high porewater pressure, generated by the loading of the ice and drainage retardation due to low permeability of the overall fine-grained sediments, decreased the shear strength and led to the original failure of the submarginal sediment and the formation of the marginal sedimentary wedge. The actual end-moraine ridge formed at the last day of the 1890 surge when the glacier became coupled to the bed and ploughed into the reverse slope of the marginal sediment wedge. The coupling was most likely caused by a drop in submarginal porewater pressure associated with porewater blow-out in front of the ice, and took place a few metres to a few tens of metres upglacier from the terminal position of the surge, as carefully estimated from the horizontal shortening within the different sections. New analysis of the structural elements within the end-moraine ridge shows that the structural evolution of the moraine ridge was more complex than previously described by Benediktsson *et al.* (2008). It is proposed that the moraine ridge developed through polyphase deformation in the sense that the phases of deformation are different (ductile, brittle) and temporally separated; ductile deformation dominated and occurred during high porewater pressures and preceded brittle deformation, which was induced when porewater pressures decreased (cf. Phillips *et al.*, 2011; Ferguson *et al.*, 2011). The formation of the moraine ridge is considered to have started with a small-scale folding and subsequent thrusting of strata which later formed the central part of the moraine ridge (Figure 8A). Subsequently, open anticline-syncline pairs formed an upper unit of lower strain as overlying strata were pushed and sheared over the central part. This interpretation is based on asymmetric box folds and sheath folds just below the anticline-syncline pair in section 1 and normal faults below the anticline in section 2. Simultaneously, the central part of the moraine deformed further, possibly obliterating some of the original deformation structures and resulting in tectonic foliation and homogenization (Figure 8B). As the ice continued to push and porewater pressures remained high, the amplitude of the original anticlines and synclines increased and they started to overturn. Thrusting occurred in the distal and proximal extremities of the moraine ridge, possibly because of a local and temporary drop in porewater pressure, as suggested by sections 1 and 2a (Figure 8C). Further pressure caused the central anticline to refold to form polyclinal overturned folds and the original synclines became deeper and narrower. New folds developed and overturned in the proximal part accompanied by thrusting. Upglacier verging anticlines began to develop in the distal extremity of the ridge due to an obstruction in front of the ridge, most likely a patch of permafrost, which generated a counter stress towards the advancing ice (Benediktsson *et al.*, 2008, 2010; Thomas and Chiverell, 2011; Figure 8D). At the very end of the surge, the system locked up as porewater pressure dropped and effective stress increased following porewater blow-out in front of the moraine ridge. This stiffened the entire wedge sequence and induced brittle deformation as seen from faults overprinting folds in sections 2 and 3, in particular (Figure 8E).

The ductile and brittle structures in the sections suggest deformation during high and low porewater pressure, respectively. Ductile deformation dominated the construction of the moraine ridge, indicating that porewater pressure in the submarginal and proglacial sediments was generally high. However, faults and shears that formed during the earlier stages of the moraine formation (e.g. section 1 and 2) suggest that porewater pressure fell slightly and temporary and locally locked the system to induce brittle deformation until porewater pressure rose again and ductile deformation continued. The greatest drop in porewater pressure occurred at the very end of the surge following a serious porewater blow out in front

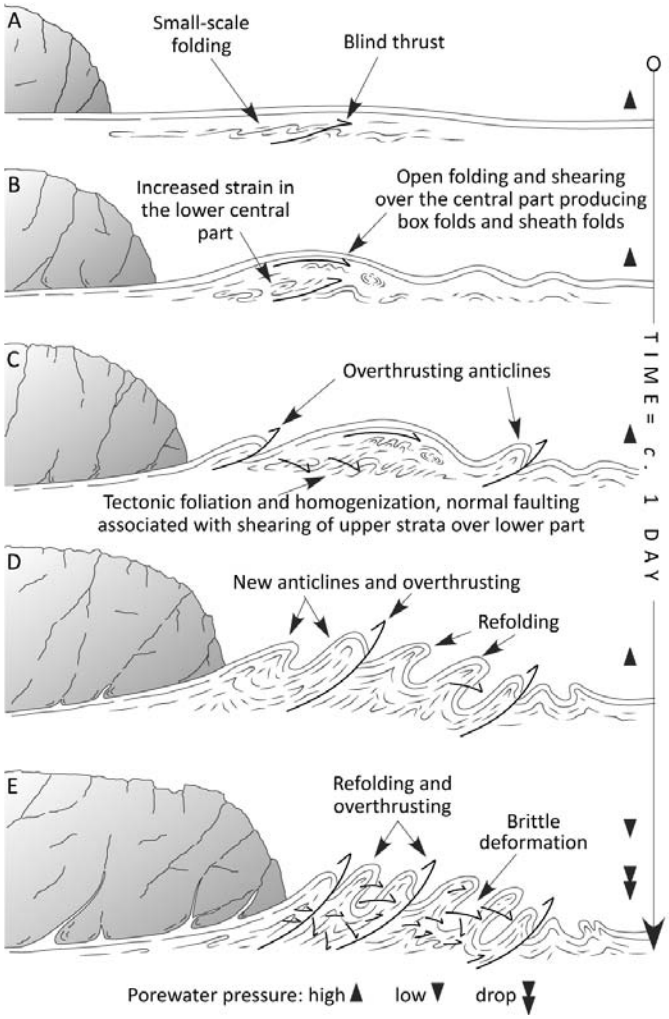

Figure 8. Model showing the polyphase structural evolution of the fine-grained, fold-dominated 1890 end moraine in Kringilsárrani. See text for details. – *Myndunarsaga jökulgarðsins sem myndaðist á síðasta degi framhlaups Brúarjökuls 1890. Líkanið sýnir hvernig fínkornótt setlögin bognuðu undan þrýstingi jökulsins og lögðust í fellingar. Fellingarnar mynduðust þegar vatnsþrýstingur í setlögunum var hár. Þegar vatnið þrýstist snögglega úr setlögunum í lok framhlaupsins, féll vatnsþrýstingurinn og þau stífnuðu og brotnuðu um skerfleti og þrýstimisgengi.*

of the moraine (Kjær *et al.*, 2006; Benediktsson *et al.*, 2008). This raised the effective stress and shear strength, causing brittle deformation as the final phase of the end-moraine formation (Figure 8).

CONCLUSIONS

The 1890 end moraine in Kringilsárrani in the central forefield of Brúarjökull was formed through polyphase deformation of overall fine-grained sediments. This is evident from different deformation styles and variable strain within four excavated cross-

sections, as exemplified by ductile and brittle deformation structures and horizontal shortening ranging from 20% to 76%.

Ductile deformation was favoured by high porewater pressure and dominated the formation of the 1890 end moraine, developing from open folding to multiple overfolding. A substantial drop in porewater pressure at the very end of the surge induced brittle deformation as the final phase of the end-moraine formation.

Folds are generally rooted indicating high friction along a basal décollement, which lies across bedrock or outwash. This suggests that the applied glaciotectonic stress was absorbed within a narrow zone, as also suggested by steeply dipping faults and axial planes of folds.

Orientation of faults and axial planes of folds primarily reflects local and marginal ice-flow direction (e.g. in an outward-spreading surge lobe) which is perpendicular to the moraine strike and not necessarily coinciding exactly with the main ice-flow direction of the 1890 surge. In general, though, structural data coincide with the ice flow from southerly directions, as expected.

Acknowledgements

Jaap van der Meer is thanked for collaboration on the 1890 end moraine in Kringilsárrani. Thanks are furthermore due to other members of the Brúarjökull field campaigns for great company and collaboration. Constructive comments by reviewers Jonathan R. Lee and Jón Eiríksson and editors Helgi Björnsson, Bryndís Brandsdóttir and Leó Kristjánsson, improved the manuscript and are gratefully acknowledged.

ÁGRIP

Rannsóknir á innri gerð jökulgarða (Hrauka) sem mynduðust við aflögun fínkornóttra setlaga í framhlaupi Brúarjökuls 1890 sýna að garðarnir urðu til á síðasta degi framhlaupsins, þegar jökullinn ýtti fram efsta og ysta hluta setfleygs sem myndast hafði undir jökulsporðinum dagana á undan. Vatnsþrýstingur í setlögunum undir og framan við jökulsporðinn var hár er þau aflögðuðust undan fargi hans; fyrst í opnar fellingar sem síðan steyptust yfir sig við aukna framrás jökulsins. Undir lok framhlaupsins þrýstist vatn út úr setlögunum og þau stífnuðu. Fellingarnar brotnuðu þá um skerfleti og þrýstimisgengi uns álaginu frá jöklinum var létt. Þetta ferli einkennir aflögun fínkornóttra setlaga við framhlaup jökla og varpar ljósi á myndun margra fornra jökulgarða.

REFERENCES

Aber, J. S. and A. Ber 2007. Glaciotectonism. Elsevier, Amsterdam. *Developm. Quaternary Sci.* 6, 1–246.

Benediktsson, Í. Ö. 2010. *End moraine and ice-marginal processes of surge-type glaciers – Brúarjökull and Eyjabakkajökull, Iceland.* Unpublished PhD. thesis, Faculty of Earth Sciences, University of Iceland, 26 pp. + 4 app.

Benediktsson, Í. Ö., P. Möller, Ó. Ingólfsson, J. J. M. van der Meer, K. H. Kjær and J. Krüger 2008. Instantaneous end moraine and sediment wedge formation during the 1890 surge of Brúarjökull, Iceland. *Quaternary Science Reviews* 27, 209–234.

Benediktsson, Í. Ö., Ó. Ingólfsson, A. Schomacker and K. H. Kjær 2009. Formation of submarginal and proglacial end moraines: implications of ice-flow mechanism during the 1963-64 surge of Brúarjökull, Iceland. *Boreas* 38, 440–457.

Benediktsson, Í. Ö., A. Schomacker, H. Lokrantz and Ó. Ingólfsson 2010. The 1890 surge end moraine at Eyjabakkajökull, Iceland, a re-assessment of a classic glaciotectonic locality. *Quaternary Science Reviews* 29, 484–506.

Benn, D. I. and D. J. A. Evans 2010. *Glaciers and Glaciation.* 2nd ed. Hodder Education, 802 pp.

Bennett, M. R. 2001. The morphology, structural evolution and significance of push moraine. *Earth-Science Reviews* 53, 197–236.

Bennett, M. R., D. Huddart, R. I. Waller, N. Cassidy, A. Tomio, P. Zukowskyj, N. G. Midgley, S. J. Cook, S. Gonzalez and N. F. Glasser 2004. Sedimentary and tectonic architecture of a large push moraine: a case study from Hagafellsjökull-Eystri, Iceland. *Sedimentary Geology* 172, 269–292.

Björnsson, H., F. Pálsson, M. T. Guðmundsson and H. H. Haraldsson 1998. Mass balance of western and northern Vatnajökull, Iceland, 1991–1995. *Jökull* 45, 35–38.

Björnsson, H., F. Pálsson and O. Sigurðsson 2003. Surges of glaciers in Iceland. *Ann. Glaciology* 36, 82–90.

Boulton, G. S., J. J. M. van der Meer, D. J. Beets, J. Hart and G. H. J. Ruegg 1999. The sedimentary and structural evolution of a recent push moraine complex: Holmstrømbreen, Spitsbergen. *Quaternary Science Reviews* 18, 339–371.

Brady, N. C. and R. R. Weil 1999. *The Nature and Properties of Soils.* Twelfth edition. Prentice Hall, New Jersey, 881 pp.

Brandes, C. and D. Le Heron 2010. The glaciotectonic deformation of Quaternary sediment by fault-propagation folding. *Proc. Geologists' Association* 121, 270–280.

Croot, D. G. 1987. Glacio-tectonic structures: a mesoscale model of thin-skinned thrust sheets? *J. Struct. Geol.* 9, 797–808.

Croot, D. G. 1988. Morphological, structural and mechanical analysis of neoglacial ice-pushed ridges in Iceland. In: Croot, D. G. (ed.), *Glaciotectonics: Forms and Processes.* Balkema, Rotterdam, 33–47.

Evans. D. J. A. and B. R. Rea 1999. Geomorphology and sedimentology of surging glaciers: a landsystem approach. *Ann. Glaciol.* 28, 75–82.

Evans, D. J. A. and B. R. Rea 2003. Surging glacier landsystem. In Evans, D. J. A. (ed.), *Glacial Landsystems.* Arnold, London, 259–288.

Evans, D. J. A. and D. I. Benn 2004. *A practical guide to the study of glacial sediments.* Arnold, London, 266 pp.

Evans, D. J. A., D. R. Twigg, B. R. Rea and M. Shand 2007. Surficial geology and geomorphology of the Brúarjökull surging glacier landsystem. *J. Maps* 2007, 349–367.

Eyles, N., C. H. Eyles and A. D. Miall 1983. Lithofacies types and vertical profile models: an alternative approach to the description and environmental interpretation of glacial diamict and diamictite sequences. *Sedimentology* 30, 393–410.

Eythorsson, J. 1963. Brúarjökull hlaupinn. (A sudden advance of Brúarjökull). *Jökull* 13, 19–21.

Eythorsson, J. 1964. Brúarjökulsleiðangur 1964. (An expedition to Brúarjökull 1964). *Jökull* 14, 104–107.

Ferguson, A., J. J. M. van der Meer and E. Phillips 2011. Micromorphology and microstructural analysis of polyphase deformation in tills: West Runton. In: Phillips, E., J. R. Lee and H. M. Evans (eds.). *Glaciotectonics – Field Guide, Quaternary Research Association*, 154–161.

French, H. 1996. *The Periglacial Environment.* Longman, Harlow, London, 341 pp.

Guðmundsson, M. T., Þ. Högnadóttir and H. Björnsson 1996. *Brúarjökull: Framhlaupið 1963-64 og áhrif þess á rennsli Jökulsár á Brú.* Raunvísindastofnun Háskólans, RH-11-96, 33 pp.

Hambrey, M. J. and D. Huddart 1995. Englacial and proglacial glaciotectonic processes at the snout of a thermally complex glacier in Svalbard. *J. Quaternary Sci.* 10, 313–326.

Huddart, D. and M. J. Hambrey 1996. Sedimentary and tectonic development of a high-arctic thrust moraine complex, Comfortlessbreen, Svalbard. *Boreas* 6, 227–243.

Humlum, O. 1985. Genesis of an imbricated push moraine, Höfðabrekkujökull, Iceland. *J. Geology* 93, 185–195.

Kjerúlf, Þ. 1962. Vatnajökull hlaupinn (Brúarjökull 1890). *Jökull* 12, 47–48.

Kjær, K. H., E. Larsen, J. J. M. van der Meer, Ó. Ingólfsson, Í. Ö. Benediktsson, C. G. Knudsen and A. Schomacker 2006. Subglacial decoupling at the sediment/bedrock interface:- a new mechanism for rapid flowing ice. *Quaternary Science Reviews* 25, 2704–2712.

Kjær, K. H., N. J. Korsgaard and A. Schomacker 2008. Impact of multiple glacier surges – a geomorphological map from Brúarjökull, East Iceland. *J. Maps*, 5–20.

Krüger, J. 1994. Glacial processes, sediments, landforms, and stratigraphy in the terminus region of Mýrdalsjökull, Iceland. *Folia Geographica Danica* 21, 1–233.

Krüger, J. and K. H. Kjær 1999. A data chart for field description and genetic interpretation of glacial diamicts and associated sediments – with examples from Greenland, Iceland, and Denmark. *Boreas* 28, 386–402.

Krüger, J., K. H. Kjær and J. J. M. van der Meer 2002. From push moraine to single-crested dump moraine during a sustained glacier advance. *Norsk Geografisk Tidsskrift* 56, 87–95.

Krüger, J., A. Schomacker and Í. Ö. Benediktsson 2010. Ice-marginal environments: Geomorphic and structural genesis of marginal moraines at Mýrdalsjökull. In: Schomacker, A., J. Krüger and K. H. Kjær (eds.). The Mýrdalsjökull Ice Cap, Iceland: Glacial processes, sediments and landforms on an active volcano. *Developm. Quaternary Sci.* 13, 79–104

Kuriger, E. M., M. Truffer, R. J. Motyka and A. K. Bucki 2006. Episodic reactivation of large-scale push moraines in front of the advancing Taku Glacier, Alaska. *J. Geophys. Res.* 111, F01009, doi:10.1029/-2005JF000385.

Maizels, J. 1993. Lithofacies variations within sandur deposits: the role of runoff regime, flow dynamics and sediment supply characteristics. *Sedimentary Geology* 85, 299–325.

Maizels, J. 2002. Sediment and landforms of modern proglacial terrestrial environments. In: Menzies, J. (ed.). *Modern and Past Glacial Environments*, revised student ed. Butterworth-Heinemann, Oxford, 279–316.

Marshak, S. and G. Mitra 1988. *Basic Methods of Structural Geology.* Prentice Hall, New Jersey, 446 pp.

McCarrol, D. and K. F. Rijsdijk 2003. Deformation styles as a key for interpreting glacial depositional environments. *J. Quaternary Science* 9, 209–233.

Motyka, R. J. and K. A. Echelmeyer 2003. Taku Glacier (Alaska, U.S.A.) on the move again: active deformation of proglacial sediments. *J. Glaciol.* 49, 50–58.

Parkes, A. A., R. I. Waller, P. G. Knight, I. G. Stimpson, D. I. Schofield and K. T. Mason 2009. A morphological, sedimentological and geophysical investigation of the Woore Moraine, Shropshire, England. *Proc. Geologists' Association* 120, 233–244.

Pedersen, S. A. S. 2005. Structural analysis of the Rubjerg Knude Glaciotectonic Complex, Vendsyssel, northern Denmark. *Geological Survey of Denmark and Greenland Bull.* 8, 1–192.

Phillips, E. and J. Merritt 2008. Evidence for multiphase water-escape during rafting of shelly marine sediments at Clava, Inverness-shire, NE Scotland. *Quaternary Science Reviews* 27, 988–1011.

Phillips, E., J. R. Lee and H. Burke 2008. Progressive proglacial to subglacial deformation and syntectonic sedimentation at the margins of Mid-Pleistocene British Ice Sheet: evidence from north Norfolk, UK. *Quaternary Science Reviews* 27, 1848–1871.

Phillips. E., J. R. Lee and H. M. Evans 2011. *Glacitectonics – Field guide*, Quaternary Res. Ass., 263 pp.

Roberts, D. H., J. C. Yde, N. T. Knudsen, A. J. Long and J. M. Lloyd 2009. Ice marginal dynamics during surge activity, Kuannersuit Glacier, Disko Island, West Greenland. *Quaternary Science Reviews* 28, 209–222.

Schomacker, A., J. Krüger and K. H. Kjær 2006. Ice-cored drumlins at the surge-type Brúarjökull, Iceland: a transitional state landform. *J. Quaternary Sci.* 21, 85–93.

Schomacker, A. and K. H. Kjær 2007. Origin and de-icing of multiple generations of ice-cored moraines at Brúarjökull, Iceland. *Boreas* 36, 411–425.

Thomas, G. S. P. 1984. The origin of the glacio-dynamic structure of the Bride Moraine, Isle of Man. *Boreas* 13, 355–364.

Thomas, G. S. P. and R. C. Chiverell 2011. Styles of structural deformation and syn-tectonic sedimentation around the margins of the Late Devensian Irish Sea Ice stram: the Isle of Man, Llyn Peninsula and County Wexford. In: Phillips, E., J. R. Lee and H. M. Evans (eds.). *Glacitectonics – Field guide, Quaternary Research Association*, 59–78.

Thorarinsson, S. 1964. On the age of the terminal moraines of Brúarjökull and Hálsjökull. *Jökull* 14, 67–75.

Thorarinsson, S. 1969. Glacier surges in Iceland, with special reference to the surges of Brúarjökull. *Canadian J. Earth Sciences* 6, 875–882.

Twiss, R. J. and E. M. Moores 1992. *Structural Geology.* W. H. Freeman and Company, New York, 532 pp.

van der Wateren, F. M. 1987. Structural geology and sedimentology of the Dammer Berge push moraine. In: J. J. M. van der Meer (ed.). *Tills and Glaciotectonics*, Balkema, Rotterdam, 157–182.

van der Wateren, D. F. M. 1995. Structural geology and sedimentology of push moraines: processes of soft sediment deformation in a glacial environment and the distribution of glaciotectonic styles. *Mededelingen Rijks Geologische Dienst*, 54 pp.

Weaver, L. and E. Arnaud 2010. Polyphase glacigenic deformation in the Waterloo Moraine, Kitchener, Ontario, Canada. *Sedimentary Geology* 235, 292–303.